Results in Engineering 15 (2022) 100584

Contents lists available at ScienceDirect

Results in Engineering

journal homepage: www.sciencedirect.com/journal/results-in-engineering

Thermosolutal natural convection energy transfer in magnetically influenced casson fluid flow in hexagonal enclosure with fillets

Imtiaz Ali Shah [a], Sardar Bilal [a], Samad Noeiaghdam [b,c,*], Unai Fernandez-Gamiz [d], Hassan Shahzad [e]

[a] Department of Mathematics, AIR University, Sector E-9, Islamabad, Pakistan
[b] Industrial Mathematics Laboratory, Baikal School of BRICS, Irkutsk National Research Technical University, Irkutsk, 664074, Russia
[c] Department of Applied Mathematics and Programming, South Ural State University, Lenin Prospect 76, Chelyabinsk, 454080, Russia
[d] Nuclear Engineering and Fluid Mechanics Department, University of the Basque Country UPV/EHU, Nieves Cano 12, 01006, Vitoria-Gasteiz, Spain
[e] Faculty of Materials and Manufacturing, College of Mechanical Engineering and Applied Electronics Technology, Beijing University of Technology, Beijing, China

ARTICLE INFO

Keywords:
Double diffusive convection
Casson fluid
Hexagonal fillet enclosure
Inclined MHD
Heat transfer
FEM

ABSTRACT

Current disquisition is aimed to adumbrate thermosolutal convective diffusion transport in Casson fluid filled in hexagonal enclosure under effectiveness of inclined magnetic field. Partially iso-concentration and iso-temperature distributions at base wall of enclosure is provided along with incorporation of fillets at corners of flow domain. Governing formulation in 2D are expressed in a velocity-pressure, energy and concentration balance equations. Numerical computations are executed by employing COMSOL Multiphysics software based on finite element scheme. Domain discretization in manifested by performing hybrid meshing in view of 2D elements. Linear and quadric interpolating polynomials for pressure and other associated distributions are capitalized. Non-linearized discretization system is handled by non-linear solver renowned as PARADISO. Results and code validation is assured by performing comparison and grid convergence test respectively. The impact of flow concerning variables by considering wide ranges like Casson parameter $(0.1 \leq \beta \leq 10)$, Rayleigh number $(10^4 \leq Ra \leq 10^7)$, Hartmann number $(20 \leq Ha \leq 80)$ and Lewis number $(0.1 \leq Le \leq 10)$ on velocity, isothermal and isoconcentration fields are visualized through graphs and tables. Visualization about kinetic energy along with heat and mass transfer rates are disclosed through graphs and tables.

1. Introduction

Fluids are driven in a domain through density variations generated by non-uniform effect of gravity at different locations. Due to production of these gradient fluid **moves** in bulk and form the procedure of convection. These changes in the density may also be caused by gradients in fluid composition or by difference in temperature and concentration distributions which is renowned as thermosolutal convection. It has received immense attention experimentally and theoretically due to superb existence in different frameworks [1–11]. In view of superb utilizations Beghein et al. [12] probed thermosolutal diffusive phenomenon in air subjected to assisting or opposing associated gradients. Gobin and Bennacer [13] conducted comprehensive work on diminution of energy transfer by enhancing magnitude of buoyancy forces. Amiri et al. [14] contemplated forced convective flow within in square enclosure under thermal and solutal differences. Nithyadevi and Yang [15] adumbrated Soret and Dufour diffusion aspects in a cavity with local heaters by. Chen et al. [16] performed computational analysis to explicate natural convection induced by heat and mass diffusions within a vertical annulus. Qin et al. [17] implemented compactly accurate finite difference scheme to attain results of convectively diffusive mixed binary liquid. Some recent efforts reported on quantification of involved physical parameters to check optimized change in double diffusion phenomenon is executed and encapsulated in Refs. [18–23]. For more studies on fluid and nanofluid flow you can see [48–51].

Liquids which behave as solid beyond certain magnitude of critical stress are known as viscoelastic materials. It is paramount to depict the strain response against application of stress to know mechanical behavior of such materials. In everyday life we are surrounded by these materials like paint, emulsions, food products, consumer products,

* Corresponding author. Industrial Mathematics Laboratory, Baikal School of BRICS, Irkutsk National Research Technical University, Irkutsk, 664074, Russia.
E-mail addresses: imtiazsha91@gmail.com (I.A. Shah), smbilal@math.qau.edu.pk (S. Bilal), snoei@istu.edu, noiagdams@susu.ru, snoei@istu.edu (S. Noeiaghdam), unai.fernandez@ehu.eus (U. Fernandez-Gamiz), hasanshahzad99@hotmail.com (H. Shahzad).

https://doi.org/10.1016/j.rineng.2022.100584
Received 22 May 2022; Received in revised form 28 July 2022; Accepted 9 August 2022
Available online 22 August 2022

concrete, waste of nuclear sludge. The study of yield stress dependent liquids has also enchanted paramount intend due to dispersed utilization in crude oil refinement, formation of plastic materials and drugs management. To depict the behavior viscoelastic liquids Casson model was presented by Casson [24] which is considered to be the fittest rheological structure possessing the characteristics of yield stress and high shearing viscosity. In recent years several studies on Casson fluid flow in different domains is taken under consideration like Rao et al. [25] described the situation due to which Casson liquid reduces to Newtonian when surface drag is greater than yield stress. Bird et al. [26] probed viscoplastic materials by determining mathematical formulation and manipulation of tensor. Latest studies related to scrutinization of non-Newtonian liquids are gathered in Refs. [27–31].

Magnetic field is implemented in transverse directions to make transport regime laminar. Such fluid which gives maximum response to the appliance of magnetic field is known as electrically conducting fluids. These liquids capture the capability of polarization and gaining charge on interaction in according with field intensity. Magnetic field implementation also plays important role in producing stratified environment in temperature production/reduction systems due to generation of buoyant forces. In addition, movement of conducting liquid in attendance of magnetic field generates addition oppositional (Lorentz) force which change the attributes in significant manner and generate addition energy storage especially in close domains. Some outstanding applications of magnetized liquids are seen in diversified engineering systems like fusion reactor designing, nuclear reactor cooling, electronic device packaging, crystal growth, solar technology. Garandet et al. [32] revealed flow and thermal characteristics of viscous liquid saturated in 2D rectangular enclosure under transversally applied magnetic field. Rudraiah et al. [33] measured decline in momentum of fluid against increasing magnitude of magnetic field due to production of Lorentzian opposing forces. He considered two magnitudes of Hartmann number i. e. $Ha = 20$ and $Ha = 100$ and also calculated Nusselt number. Hadid et al. [34] developed dimensionless expression of Hartmann number by using scale analysis for fluid flow in confined geometries. Piazza and Ciofalo [35] analyzed heat and flow characteristics versus Hartmann numbers varied between 100 and 1000. Oztop [36] numerically simulated magnetically influenced flow of nanoliquid in wavy cavity. Fatih et al. [37] quantitatively analyzed convective energy transport in different liquids enclosed in cavity with a corrugation. Thermal characteristics about magnetized pulsating flow along with induction of nanoparticles and effectiveness of surface corrugation in bifurcating channel was examined by Selimefendigil et al. [38]. Convection heat transfer in different shaped enclosure has been investigated in Refs. [39–47].

From the overview of aforementioned scientific research, it is evaluated that thermosolutal diffusive mechanism in liquids has not yet been interrogated. In addition, overwhelming emergence regarding diffusive convective transport in enclosures is found such as indoor energy management, cooling of shafts, lubrications of bearings and food processing. So, the motive behind this disquisition is to fill this gap by examining heat and mass transport in Casson non-Newtonian liquid with provision of isothermal and isoconcentration profiles at bottom wall and at surface of cylinder.

Current document is organized in following structuring firstly, literature survey regarding considered fluid model and physical aspects is carried out, then secondly formulation of problem is presented, thirdly the steps involved in computational scheme are presented, afterward outcomes and discussion are disclosed and at last conclusion of study are displayed.

2. Mathematical modelling

2.1. Problem definition

We have considered 2D, steady, incompressible and laminarly flow of Casson liquid filled in hexagonal cavity with inner circular cylinder. Density of fluid is assumed to be impersistent and formulated by Boussinesq approach along with consideration of shear rate dependent viscosity. Uniform temperature (T_h) and concentration (C_h) is provided at bottom extremity and surface of circular cylinder whereas upper boundary is under the influences of cooled temperature (T_c) with constant concentration (C_c). Inclined magnetic field of strength B is employed to domain making angle of γ. The schematic representation of domain is shown in Fig. 1.

2.2. Governing equations

The constitutive equations in dimensional form on basis of above assumptions is presented as follows [47]:

$$\frac{\partial u}{\partial x}+\frac{\partial v}{\partial y}=0, \tag{1}$$

$$\rho\left(u\frac{\partial u}{\partial x}+v\frac{\partial u}{\partial y}\right)=-\frac{\partial p}{\partial x}+\mu\left(1+\frac{1}{\beta}\right)\left(\frac{\partial^2 u}{\partial x^2}+\frac{\partial^2 u}{\partial y^2}\right)+\Lambda_x, \tag{2}$$

$$\rho\left(u\frac{\partial v}{\partial x}+v\frac{\partial v}{\partial y}\right)=-\frac{\partial p}{\partial x}+\mu\left(1+\frac{1}{\beta}\right)\left(\frac{\partial^2 v}{\partial x^2}+\frac{\partial^2 v}{\partial y^2}\right)+\Lambda_y, \tag{3}$$

$$u\frac{\partial T}{\partial x}+v\frac{\partial T}{\partial y}=\alpha_e\left(\frac{\partial^2 T}{\partial x^2}+\frac{\partial^2 T}{\partial y^2}\right), \tag{4}$$

$$u\frac{\partial c}{\partial x}+v\frac{\partial c}{\partial y}=D\left(\frac{\partial^2 c}{\partial x^2}+\frac{\partial^2 c}{\partial y^2}\right), \tag{5}$$

where (u,v) are the velocity components along the (x,y), while ρ, μ, β, α_e, D, p are fluid density, kinematic viscosity, Casson parameter, thermal diffusivity, diffusion coefficient, pressure respectively and $\Lambda = (\Lambda_x, \Lambda_y)$ shows the force index due to magnetic field.

The force index generated in view of Lorentz force and temperature and concentration gradients formulated by employing Boussinesq approximation is expressed as follows

$$\Lambda_x=\sigma B_0^2\left(v\sin\gamma\cos\gamma-u\sin^2\gamma\right) \tag{6}$$

$$\Lambda_y=\sigma B_0^2\left(u\sin\gamma\cos\gamma-v\cos^2\gamma\right)+\rho g[\beta_T(T-T_c)+\beta_c(c-c_c)] \tag{7}$$

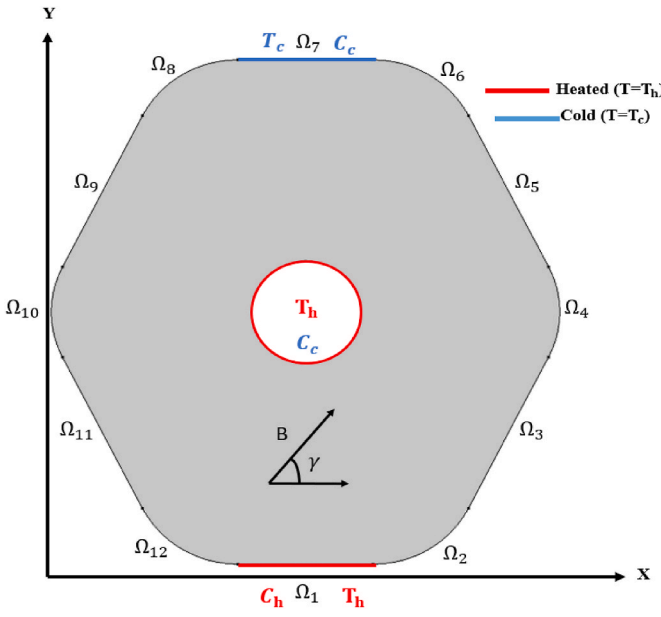

Fig. 1. Diagrammatic representation of the problem.

where, β_T and β_c show the thermal and solutal expansions, respectively.

2.3. Boundary constraints

$$u=0,\ v=0,\ T=T_h,\ c=c_h\ (\text{Hot side}) \tag{8}$$

$$u=0,\ v=0,\ T=T_c,\ c=c_c\ (\text{Cold side}) \tag{9}$$

$$u=0,\ v=0,\ \frac{\partial T}{\partial n}=\frac{\partial c}{\partial n}=0,\ (\text{Remaining walls}) \tag{10}$$

where n shows the normal vector on the boundary.

Following parameters are utilized for conversion of governing equations into non-dimensional form.

$$(X^*,Y^*)=\frac{(x,y)}{L},\ (U^*,V^*)=\frac{(u,v)L}{\alpha},\ P^*=\frac{pL^2}{\rho\alpha^2},\ \theta^*=\frac{T-T_c}{T_h-T_c},\ C^*=\frac{c-c_c}{c_h-c_c} \tag{11}$$

$$\alpha_e=\frac{k_e}{(\rho c_p)_f},\ Ra=\frac{\rho^2\beta_T g L^3\Delta TPr}{\upsilon^2},\ Le=\frac{\alpha_e}{\mathrm{D}},\ Ha=BL\sqrt{\frac{\mu}{\sigma}},\ Pr=\frac{\nu}{\alpha}. \tag{12}$$

Following non-dimensional representation of governing equations is obtained

$$\frac{\partial U^*}{\partial X^*}+\frac{\partial V^*}{\partial Y^*}=0 \tag{13}$$

$$\left(U^*\frac{\partial U^*}{\partial X^*}+V^*\frac{\partial U^*}{\partial Y^*}\right)=-\frac{\partial P^*}{\partial X^*}+Pr\left(1+\frac{1}{\beta}\right)\left(\frac{\partial U^*}{\partial X^*}+\frac{\partial U^*}{\partial Y^*}\right)+\Lambda_{X^*} \tag{14}$$

$$\left(U^*\frac{\partial V^*}{\partial X^*}+V^*\frac{\partial V^*}{\partial Y^*}\right)=-\frac{\partial P^*}{\partial Y^*}+Pr\left(1+\frac{1}{\beta}\right)\left(\frac{\partial V^*}{\partial X^*}+\frac{\partial V^*}{\partial Y^*}\right)+\Lambda_{Y^*}, \tag{15}$$

$$U^*\frac{\partial\theta^*}{\partial X^*}+V^*\frac{\partial\theta^*}{\partial Y^*}=\frac{\partial^2\theta^*}{\partial X^{*2}}+\frac{\partial^2\theta^*}{\partial Y^{*2}}, \tag{16}$$

$$U^*\frac{\partial C^*}{\partial X^*}+V^*\frac{\partial C^*}{\partial Y^*}=\frac{1}{Le}\left(\frac{\partial^2 C^*}{\partial X^{*2}}+\frac{\partial^2 C^*}{\partial Y^{*2}}\right), \tag{17}$$

where,

$$\Lambda_{X^*}=PrHa^2\left(V^*sin\gamma cos\gamma-U^*sin^2\gamma\right) \tag{18}$$

$$\Lambda_{Y^*}=PrHa^2\left(U^*sin\gamma cos\gamma-V^*cos^2\gamma\right)+RaPr(\theta^*+NC^*) \tag{19}$$

Associated boundary conditions in dimensionless form

$$U^*=0,\ V^*=0,\ \theta^*=1,\ C^*=1\ (\text{Hot side}) \tag{20}$$

$$U^*=0,\ V^*=0,\ \theta^*=0,\ C^*=0\ (\text{cold side}) \tag{21}$$

$$U^*=0,\ V^*=0,\ \frac{\partial\theta^*}{\partial n}=\frac{\partial C^*}{\partial n}=0\ (\text{Remaining walls}) \tag{22}$$

Mathematical relations for local and average heat fluxes are defined as under

$$Nu_{local}=\left(-\frac{\partial\theta^*}{\partial X^*}\right)_{X^*=0} \tag{23}$$

$$Sh_{local}=\left(-\frac{\partial C^*}{\partial X^*}\right)_{X^*=0} \tag{24}$$

$$Nu_{avg}=\frac{1}{S}\int_S^1 Nu_{local}\,dS \tag{25}$$

$$Sh_{avg}=\frac{1}{S}\int_S^1 Sh_{local}\,dS. \tag{26}$$

Additionally, global quantity, namely the total kinetic energy is expressed as under

$$K.E=\frac{1}{2}\int_\Omega U^2\ \mathrm{d}\Omega \tag{27}$$

where $U=(U^*,\ V^*)$ is the velocity vector.

3. Solution methodology

Fluid flow behavior in non-confined boundaries is easily handled by way of exact approaches but extracting the solution in closed enclosure along with various shapes of obstacle is difficult with the help of traditional methods. So, most of the researchers utilize numerical schemes to report the findings and most generous methods are FDM, FEM and FVM. Among these mentioned numerical methodologies finite element scheme is a versatile method because of the fact that the modelling of complex and irregular shapes is easily handled by discretizing the available domain with finite elements. We have utilized the stable quadratic elements for the computations of velocity and temperature whereas the pressure is approximated through linear elements. In present pagination a hybrid finite element mesh is used consisting of rectangular and triangular elements. The computational mesh at coarse grid level is disclosed in Fig. 2 and the corresponding degrees of freedom at further refinement levels are shown in Table 1. Steps involving in finite element method are mentioned in Fig. 3. In FEM Newton's scheme is capitalized for linearization of non-linearized expressions and resulting linear system of equations is heeded through a direct solver based on elimination with special rearrangement of unknowns. The following convergence criterion is set for the nonlinear iterations

$$\left|\frac{\chi^{n+1}-\chi^n}{\chi^{n+1}}\right|<10^{-6}$$

where, χ characterizes the general solution component.

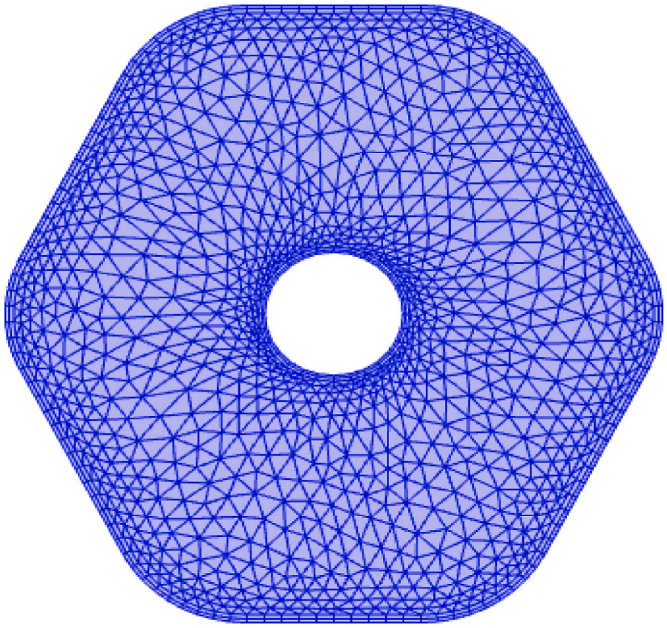

Fig. 2. Coarse grid for cavity with a circular block placed at C (0.5,0.5).

Table 1
Mesh statistics for various refinement levels.

Grid	# EL	#DOFs
1	390	2607
2	552	3630
3	878	5643
4	1476	9284
5	2130	13,189
6	3388	20,504
7	8092	48,224
8	20,002	117,161
9	27,678	159,379

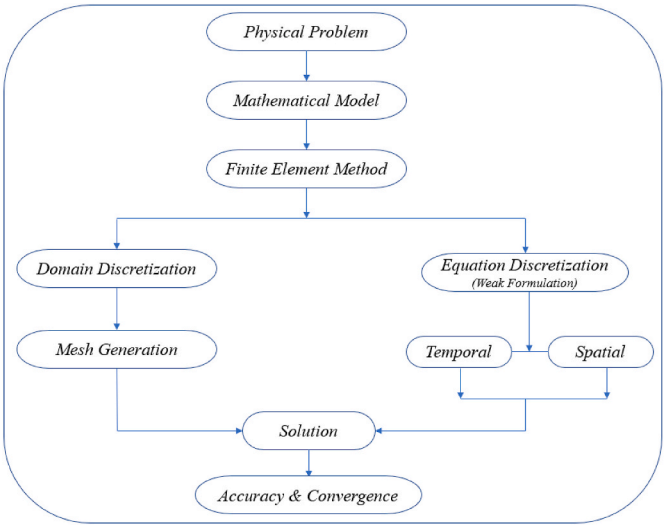

Fig. 3. Schematic diagram of finite element method.

3.1. Grid convergence

To show credibility of capitalized numerical scheme grid convergence test is performed at various grids levels and by restricting $\beta = 1$, $Ha = 25$, $Le = 2.5$, $Pr = 6.8$, *and* $Ra = 10^5$ and are shown in Table 2. For this purpose, average heat and mass fluxes are computed along with kinetic energy is estimated. It is seen that at level 8 and 9 the values of mentioned quantities of engineering interest shows agreement with each other.

3.2. Validation of results

Assurance of results is done by making agreement with finding published by Shafqat et al. [47] by computing average Nusselt number against Casson fluid parameter β and fixing $Ha = 25$, Le, 2.5, $Pr = 6.8$, $Ra = 10^5$ as shown in Table 3. From attained data a complete match is found among the results.

Table 2
Grid convergence study for average heat and mass fluxes.

Grid	Nu_{avg}	Sh_{avg}	K.E.
1	3.75363136	5.68512734	270.48422976
2	3.81369224	5.81912339	261.06388315
3	3.82877393	5.88188671	250.70895835
4	3.83572803	5.92201758	245.15826789
5	3.83140013	5.92086826	242.53478270
6	3.82878385	5.92695777	240.29134435
7	3.81880973	5.93139327	237.70263738
8	3.81168274	5.92048017	236.55162873
9	3.81111887	5.92046308	236.27636230

Table 3
Agreement of results with Shafqat et al. [47] against different value of.β.

β	Shafqat et al. [25]	Present
0.1	2.38986	2.39023
1	3.81194	3.81168
5	4.27587	4.27511
10	4.35556	4.35470

4. Result and description

This segment is offered to interpret accomplished outcomes in view of stream lines, isotherms and isoconcentration patterns against sundry parameters like (β), (Ra), (Le) and (Ha). Additionally, quantities like heat and mass fluxes, kinetic energy are also measured. In addition, for getting optimized variation in flow distributions some parametric variables are assigned with specific values i.e. heat capacity $(c_p = 1)$, isotropic thermal conductivity $(k = 1)$, density $(\rho = 1)$ and ratio specific heat. $(\gamma = 1)$.

The effectiveness of Casson parameter (β) on momentum, temperature and concentration distributions are revealed in Fig. 4(a–c). Fig. 4(a) exclusively discusses change in velocity distribution via stream lines against (β). Intensification in strength of stream lines is adhered at lower magnitude of (β) whereas opposite trend is observed at $\beta = 10$. It is because of the fact that at higher magnitude of (β) viscosity of fluid increases but because the appearance of (β) is in reciprocal form in momentum equation so by increasing (β) velocity enhances due to which momentum of fluid reduces. Additionally, it is also observed that by increasing (β) intensity of fluid in portion lying lower to obstacle is lesser than upper portion which is evidenced from stream line patterns. Change in thermal field against Casson parameter (β) is divulged in Fig. 4(b). It is disclosed that at $(\beta) = 10$ isotherms magnitude attain greater response because at higher β velocity of liquid as well as average kinetic energy mounts and temperature profile represents positive tend. Here, in isotherm two different regions are formed one below the cylinder in which it is explicitly seen that heat transfer increases where as in lower region different shapes of thermal trajectories are attained. It is worthwhile to mention that heat is transferred from lower portion of enclosure to higher due to placement of localized heat source at bottom wall and production of convective thermal potential. Fig. 4(c) discloses the impact of Casson fluid parameter (β) on concentration field. It is seen that at lower magnitude of (β) less dispersion in fluid particles is generated and thus as an outcome concentration of fluid enhances which is proved by formation of arched shaper isoconcentration contours. Whereas, at higher magnitude of (β) Casson fluid approaches towards Newtonian behavior and viscosity of fluid decays thus more disturbance in fluid is produced which causes reduction in concentration field. Since, in the present work concentration buoyancy forces are generated by providing uniform concentration at base wall and providing zero concentration at cylinder. It is depicted that by at lower magnitude of (β) viscosity is maximum and fluid molecule accumulates near the base wall. In addition, squeezing of region at higher magnitude of (β) is observed.

Fig. 5(a–c) illustrates the change in magnitude of stream lines, isotherms, isoconcentrations against (Ra) ranging from $Ra = 10^5 - 10^7$. In Fig. 5(a) it is manifested that magnitude of stream function interpreted in the form of stream lines mounts against increasing magnitude of Rayleigh number (Ra). It is justified by mathematical relation existing for dimensionless coefficient of Rayleigh number i.e. $Ra = \frac{\rho^2 \beta_T g L^3 \Delta T Pr}{\nu^2}$. From this expression it is seen that with uplift in (Ra) viscosity of fluid decreases because (Ra) has inverse relation with viscous forces. It is salient to mention that four vortices are formed and deviation in structuring of stream lines appear at higher magnitude of (Ra). Subsequently, it is also manifested that direction of movement of fluid in upper and lower halves are opposite to each other. Fig. 5(b) expresses change in temperature distribution against (Ra) via isotherm patterns. It

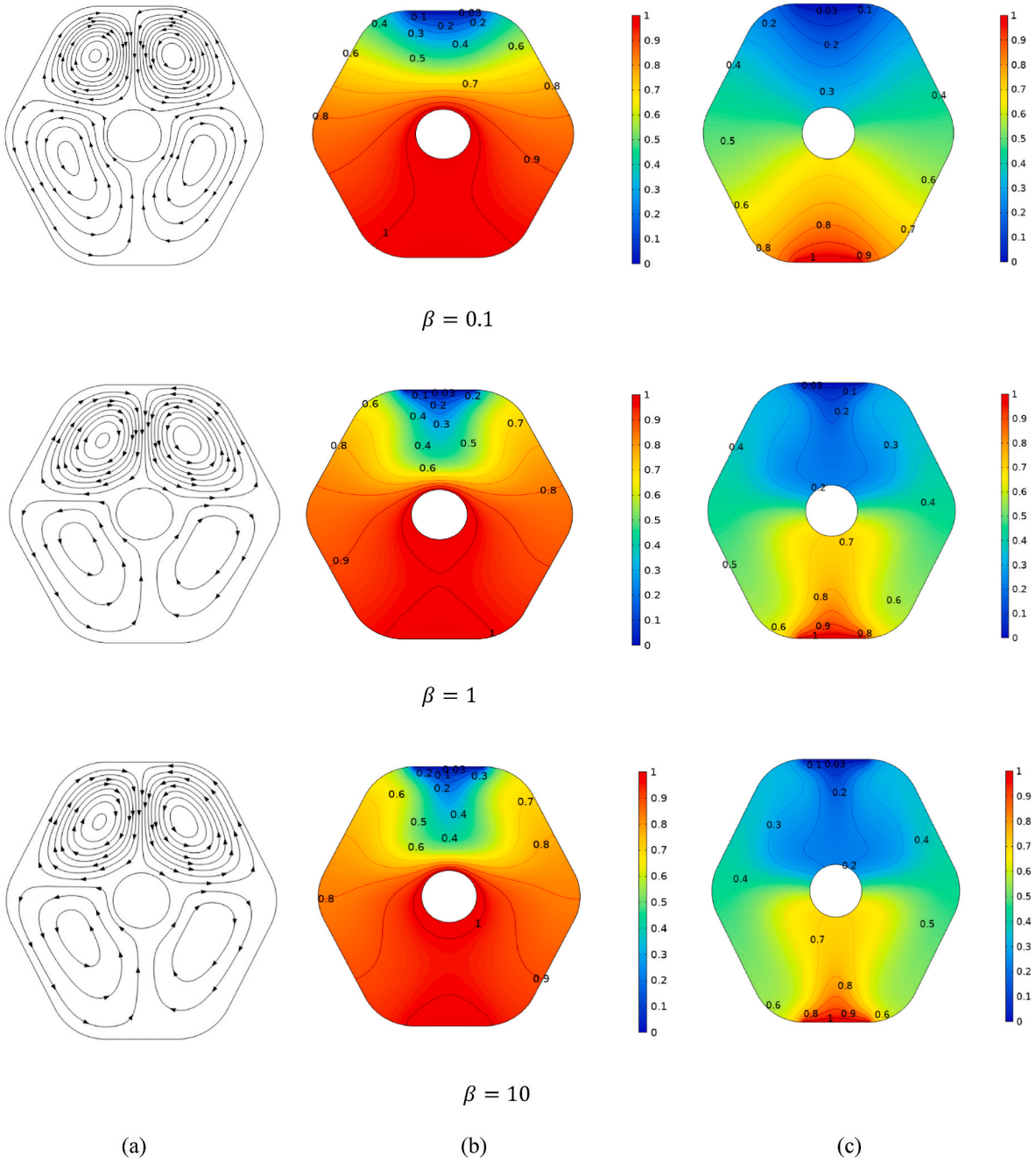

Fig. 4. (a–c) Deviation in momentum, thermal and solutal profiles against (β).

is observed that by increasing magnitude of (Ra) temperature of fluid enhances which is validated by isothermal contour patterns. This fact is justified by the relation that by increasing (Ra) temperature difference between hot and cold regions rises and thermal buoyancy forces are produced because (Ra) is directly proportional ΔT . So, at $Ra = 10^7$ maximum diffusion of temperature distribution is revealed and region above the cylinder widened. Change in concentration profile against Rayleigh number (Ra) is divulged in Fig. 5(c). It is adhered that at lower magnitude of (Ra) concentration of fluid is more than in case of higher magnitude of (Ra). The reason behind this behavior is that at lower values of (Ra) i.e. $Ra = 10^5$ low solutal convective potential is produced due to less concentration difference and fluid accumulates and concentration field uplifts.

In Fig. 6 we investigated the effect of Lewis number (*Le*) varying from 0.1 *to*10 on momentum, temperature and concentration distributions. Fig. 6(a) interprets variation in velocity behavior against Lewis number (*Le*). No significant changes in momentum distribution is observed against (*Le*) because it has no direction relation with momentum diffusivity. Fig. 6(b) shows upshot of Lewis number (*Le*) on isothermal contours by fixing $Pr = 6.8$, $Ha = 25$, $\beta = 1$, $Ra = 10^5$, $N = 1$, $\gamma = 1$. Likewise, the velocity profile there is no apparent change in temperature distribution is observed against (*Le*). Positive trend in magnitude of mass flux is scrutinized against (*Le*) in Fig. 6(c). Since, Lewis number (*Le*) represents the ratio of thermal to mass diffusivities so by increasing (*Le*) the thermal diffusion elevates whereas mass diffusivity declines. Thus, at $Le = 0.1$ optimized region is attained due to less mass diffusion and at $Le = 10$ thinner region of isoconcentration is seen.

Fig. 7(a–c) illustrates change in velocity, temperature and concentration distributions against incrementing magnitude of magnetic field parameter (*Ha*). Since, Hartmann number (*Ha*) is involved in present

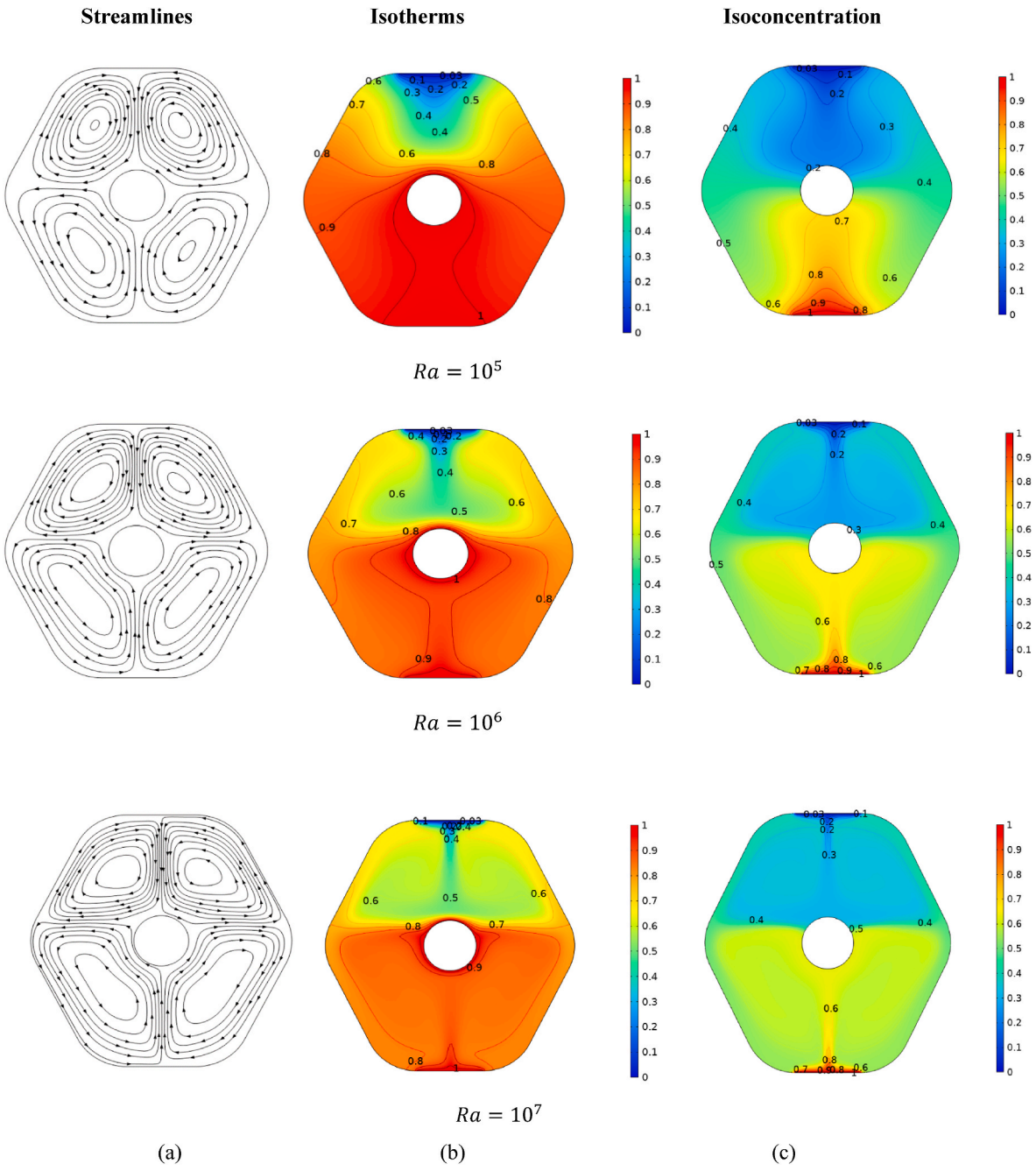

Fig. 5. (a–c). Deviation in momentum, thermal and solutal profiles against (*Ra*).

study due to incorporation of magnetic field which has role in reducing velocity profile and making the flow regime laminar. Fig. 7(a) explains the flow behavior of Casson liquid in hexagonal structure against appliance of Hartmann number (*Ha*). Lower magnitude of velocity is attained at $Ha = 60$ and maximum value of velocity distribution is received at $Ha = 20$. It is because of the fact that due to strength of Hartmann number (*Ha*) produces opposing Lorentz force which causes resistance to fluid and ceases the motion. Fig. 7(b) perceives deviation in thermal distribution in view of isothermal contours against Hartmann number (*Ha*). As Hartmann number (*Ha*) shows ratio of $Ha = BL\sqrt{\frac{\mu}{\sigma}}$ in which it is observed that viscosity of fluid enhances against (*Ha*) due to which average kinetic energy of fluid diminishes and thus as an outcome temperature distribution decay. Enhancement in concentration distribution with increase in Hartmann number (*Ha*) is observed in Fig. 7(c). It is because by increasing (*Ha*) viscosity enriches due to which concentration of fluid mounts. In addition, more dominating isoconcentration region is produced at $Ha = 60$.

Table 4 represent numerical data regarding change in average Nusselt number Nu_{avg} and average Sherwood number (Sh_{avg}) against Hartmann number (*Ha*) and Casson fluid parameter (β) with fixation of Pr = 6.8, Ra = 105, $Le = 2.5$, N = 1, $\gamma = 30°$. As observed, the highest mean Nusselt number and Sherwood number was occurred in $\beta = 10$ and $Ha = 0$ with magnitude 1.9596 and 1.4221 respectively. At $Ha = 0$ there is no magnetic field thus the resistive forces are absent due to this factor velocity as well as kinetic energy is at high magnitude and temperature flux enhances. The reason for increasing behavior of average heat and mass fluxes is that by increasing Casson parameter (β) fluid approaches towards Newtonian behavior and viscosity of fluid reduces due to which kinetic energy exceeds and both mentioned flux rates enhance. Whereas, contrary behavior is observed in average heat and mass fluxes against

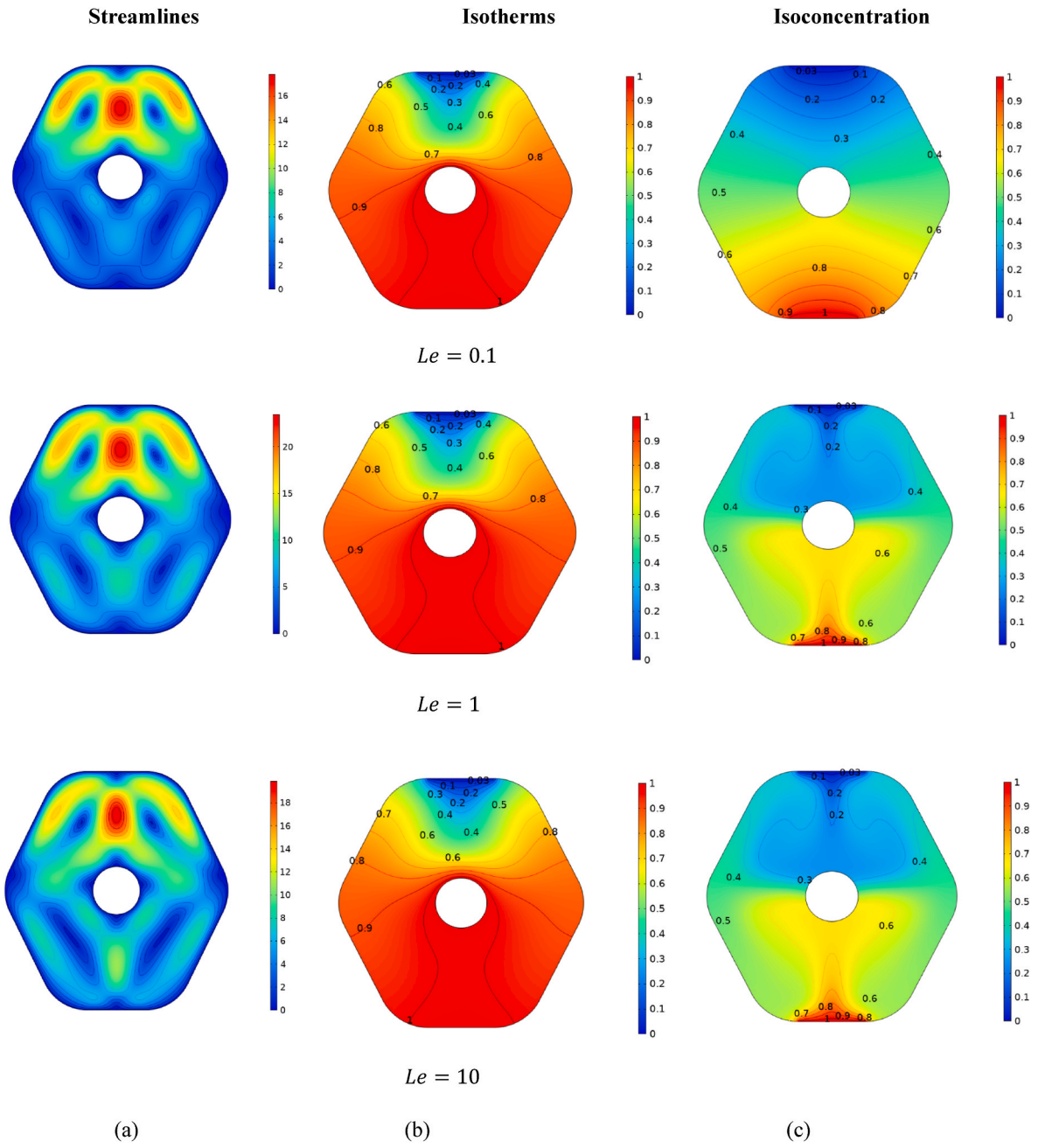

Fig. 6. (a–c). Deviation in momentum, thermal and solutal profiles against (*Le*).

Hartmann number (*Ha*). This fact is proved by the production of resistive forces in flow domain due to enhancement of (*Ha*) along with reduction in kinetic energy of particles as well.

Table 5 demonstrates variation in average kinetic energy for different values of Hartmann number (*Ha*) and Casson parameter (β). The results exhibited that the kinetic energy at $\beta = 10$ and $Ha = 0$ was increased 13.2 times more than for $\beta = 0.1$ and $Ha = 0$. It is seen that by increasing Casson parameter (β) Casson fluid behaves like Newtonian fluid because as $\beta \to \infty$ Casson fluid becomes Newtonian fluid due to which viscosity of fluid reduces. This reduction in viscosity elevates the motion of fluid along with uplift in kinetic energy. Whereas, decrementing aptitude in kinetic energy is observed against Hartmann number (*Ha*) due to generation of Lorentz forces which offers resistance to motion of fluid particles and restricts increment in kinetic energy.

5. Concluding remarks

Double Diffusive Natural Convection regime in Casson fluid flow in hexagonal enclosure for uniform thermal and concentration distributions and by placing heated and concentrated cylinder is analyzed in current communication. Fillets used at corners of enclosure to remove singularities formation in the computational domain. Mathematical formulation of problem by capitalizing governing law is executed in the form of dimensionless partial differential system. Numerical simulations are performed by implementing finite element procedure. Variation in associated momentum, temperature and concentration distributions in view of steam lines, isothermal and isoconcentration patterns are disclosed. Quantities of engineering interest like kinetic energy, local heat and mass flux coefficients is also measured against dimensionless involved physical parameters. Key findings of current analysis are enlisted below.

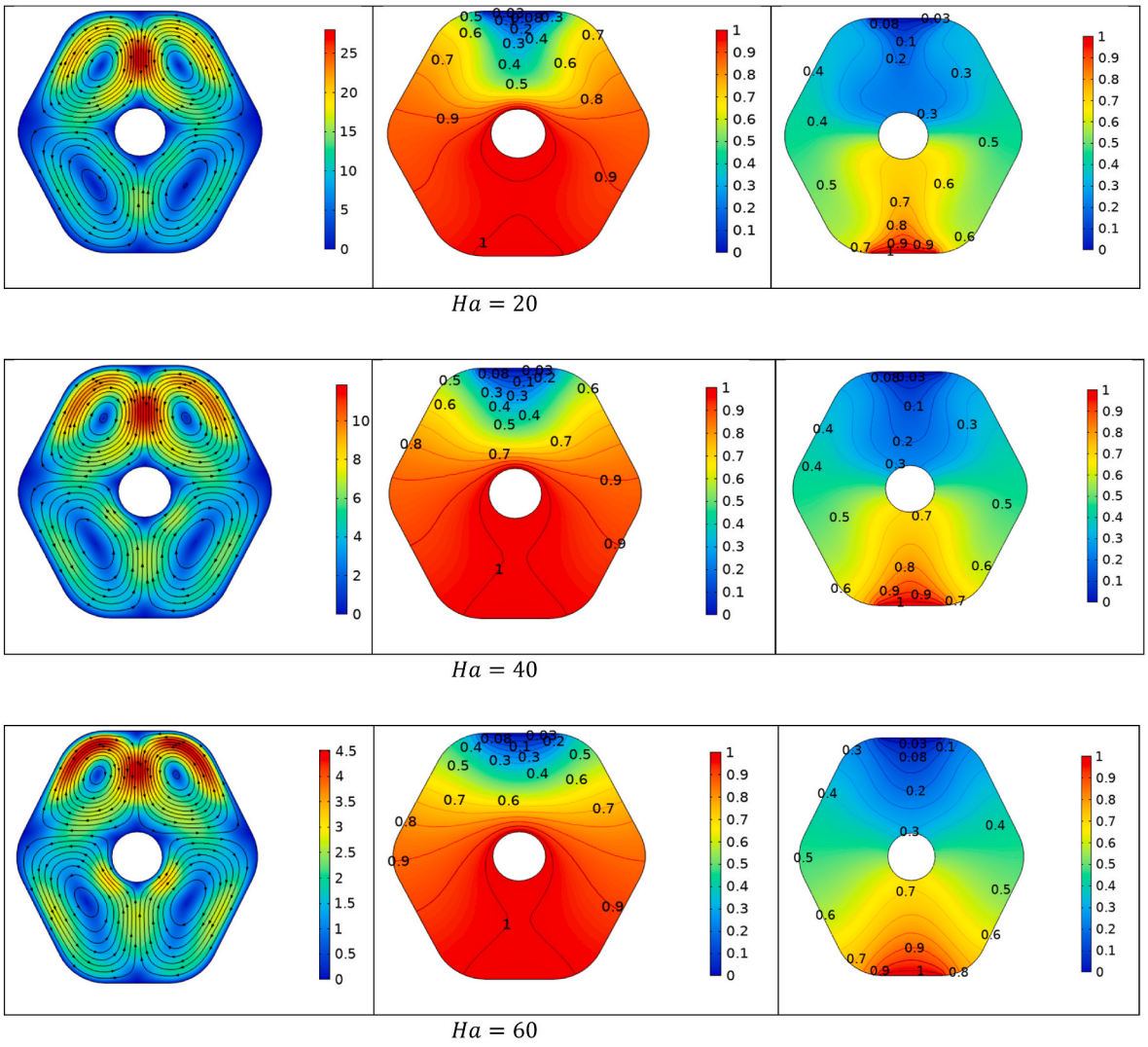

Fig. 7. (a–c). Deviation in momentum, thermal and solutal profiles against (*Ha*).

Table 4
Variation of average Nusselt number and Sherwood numbers against Casson parameter (β) and Hartmann number (*Ha*).

Nu_{avg}				Sh_{avg}		
Ha	$\beta = 0.1$	$\beta = 1$	$\beta = 10$	$\beta = 0.1$	$\beta = 1$	$\beta = 10$
0	1.565584	1.678796	1.959645	0.758038	1.221762	1.422147
25	1.556878	1.673649	1.958622	0.753727	1.214584	1.413668
50	1.531793	1.658796	1.955704	0.741143	1.193234	1.388552
75	1.493206	1.635878	1.95132	0.721378	1.158268	1.347703
100	1.445228	1.607266	1.946108	0.696323	1.110596	1.292422

Table 5
Variation of average kinetic for various values of Casson parameter (β) and Hartmann number (*Ha*).

K.E			
Ha	$\beta = 0.1$	$\beta = 1$	$\beta = 10$
0	4.427129	29.29098	57.70366
25	4.328288	28.6671	56.2963
50	4.045391	26.88837	52.33967
75	3.617216	24.20405	46.52324
100	3.101223	20.94784	39.71034

- By increasing Lewis number (*Le*) mass distribution reduces justified by isoconcentration pattern.
- Temperature distribution enhances whereas concentration profile depreciates against increasing magnitude of Rayleigh number (Ra).
- Intensification in kinetic energy is revealed against (*Ha*) whereas contrary attribute is observed against (β).
- Heat and mass flux coefficients show diminishing aspects against Hartmann number (*Ha*).
- Against Casson parameter (β) heat and mass flux distribution show upsurging behavior.

- Uplift in temperature distribution and contrary behavior in concentration profile is depicted against incrementing values of Hartmann number.
- Due to consideration of heat and concentrated circular cylinder extensive heat and mass diffusions are measured in its vicinity.
- Rayleigh number (Ra) plays influential role in convective heat and mass transfer.

Credit author statement

Imtiaz Ali Shah: Conceptualization; Data curation; Formal analysis; Investigation; Methodology; Resources; Software; Validation; Visualization; Roles/Writing – original draft; Writing – review & editing. **Sardar Bilal**: Conceptualization; Data curation; Formal analysis; Investigation; Methodology; Supervision; Resources; Software; Validation; Writing – original draft; Writing – review & editing. **Samad Noeiaghdam**: Formal analysis; Funding acquisition; Investigation; Methodology; Project administration; Resources; Supervision; Writing – review & editing. Unai Fernandez-Gamiz: Formal analysis; Funding acquisition; Investigation; Methodology; Project administration; Resources; Software; Validation; Writing – review & editing. **Hassan Shahzad**: Conceptualization; Formal analysis; Methodology; Resources; Software; Validation; Visualization; Writing – review & editing. The authors read and confirmed the authorship.

Funding

The work of U·F.-G. was supported by the Government of the Basque Country for the ELKARTEK21/10KK-2021/00014 and ELKARTEK22/85 research programs, respectively.

Declaration of competing interest

The authors declare that they have no known competing financial interests or personal relationships that could have appeared to influence the work reported in this paper.

Nomenclature

x	Horizontal coordinate (dimensional), m
y	vertical coordinate (dimensional), m
u	x-coordinate velocity (dimensional), m/s
v	y-coordinate velocity(dimensional), m/s
Le	Lewis number, $\left(\frac{\alpha_e}{\mathrm{D}}\right)$
Pr	Prandtl number, $\left(\frac{\nu}{\alpha}\right)$
g	Gravitational acceleration, m/ s^2
Ra	Rayleigh number, $\left(\frac{\rho^2\beta_T g L^3 \Delta T Pr}{\mu^2}\right)$
Ha	Hartmann number, $\left(BL\sqrt{\frac{\mu}{\sigma}}\right)$
c	Concentration (dimensional)
$\boldsymbol{B}_0$	Magnetic field strength
μ	Dynamic viscosity, Ns/ m^2
T	Temperature (dimensional), K
P	fluid pressure (dimensional), Pa
k_e	Thermal conductivity (effective)
α_e	Thermal diffusivity (effective)
Nu	Nusselt number (local)
C_p	Specific heat, J/kg. K
Sh	Sherwood number(local)

Greek Symbols

$\boldsymbol{\theta}$	Temperature (dimensionless)
$\boldsymbol{\rho}$	Fluid density, kg/ $\boldsymbol{m}^3$
$\boldsymbol{\beta}$	Casson fluid parameter

References

[1] G.H.R. Kefayati, H. Tang, Three-dimensional Lattice Boltzmann simulation on thermosolutal convection and entropy generation of Carreau-Yasuda fluids, Int. J. Heat Mass Tran. 131 (2019) 346–364.
[2] Shihe Xin, Patrick Le Quéré, Laurette S. Tuckerman, Bifurcation analysis of double-diffusive convection with opposing horizontal thermal and solutal gradients, Phys. Fluids 10 (1998) 850–858.
[3] I. Sezai, A.A. Mohamad, Double diffusive convection in a cubic enclosure with opposing temperature and concentration gradients, Phys. Fluids 12 (2000) 2210–2223.
[4] Geniy V. Kuznetsov, Mikhail A. Sheremet, A numerical simulation of double-diffusive conjugate natural convection in an enclosure, Int. J. Therm. Sci. 50 (2011) 1878–1886.
[5] Lyes Khezzar, Dennis Siginer, Igor Vinogradov, Natural convection of power law fluids in inclined cavities, Int. J. Therm. Sci. 53 (2012) 8–17.
[6] Ali, Liaqat, Bagh Ali, Xiaomin Liu, Shehzad Ahmed, and Murad Ali Shah. "Analysis of bio-convective MHD Blasius and Sakiadis flow with Cattaneo-Christov heat flux model and chemical reaction." Chin. J. Phys. 77 (2022): 1963-1975.
[7] Herbert E. Huppert, J. Stewart Turner, Double-diffusive convection, J. Fluid Mech. 106 (1981) 299–329.
[8] Simon Ostrach, Fluid mechanics in crystal growth-the 1982 freeman scholar lecture, ASME J. Fluids Eng. 105 (1983) 5–20.
[9] Raymond W. Schmitt, Double diffusion in oceanography, Annu. Rev. Fluid Mech. 26 (1) (1994) 255–285.
[10] Timour Radko, Double-diffusive Convection, Cambridge University Press, 2013.
[11] Massimo Corcione, Stefano Grignaffini, Alessandro Quintino, Correlations for the double-diffusive natural convection in square enclosures induced by opposite temperature and concentration gradients, Int. J. Heat Mass Tran. 81 (2015) 811–819.
[12] C. Beghein, F. Haghighat, F. Allard, Numerical study of double-diffusive natural convection in a square cavity, Int. J. Heat Mass Tran. 35 (1992) 833–846.
[13] D. Gobin, R. Bennacer, Cooperating thermosolutal convection in enclosures—II. Heat transfer and flow structure, Int. J. Heat Mass Tran. 39 (1996) 2683–2697.
[14] Abdalla M. Al-Amiri, Khalil M. Khanafer, Ioan Pop, Numerical simulation of combined thermal and mass transport in a square lid-driven cavity, Int. J. Therm. Sci. 46 (2007) 662–671.
[15] Pengwei Zhou, Yunbo Zhong, Huai Wang, Lijun Fan, Licheng Dong, Li Fu, Qiong Long, Tianxiang Zheng, Behavior of Fe/nano-Si particles composite electrodeposition with a vertical electrode system in a static parallel magnetic field, Electrochim. Acta 111 (2013) 126–135.

[16] Sheng Chen, Tölke Jonas, Manfred Krafczyk, Numerical investigation of double-diffusive (natural) convection in vertical annuluses with opposing temperature and concentration gradients, Int. J. Heat Fluid Flow 31 (2010) 217–226.
[17] Q. Qin, Z.A. Xia, Zhen F. Tian, High accuracy numerical investigation of double-diffusive convection in a rectangular enclosure with horizontal temperature and concentration gradients, Int. J. Heat Mass Tran. 71 (2014) 405–423.
[18] Massimo Corcione, Stefano Grignaffini, Alessandro Quintino, Correlations for the double-diffusive natural convection in square enclosures induced by opposite temperature and concentration gradients, Int. J. Heat Mass Tran. 81 (2015) 811–819.
[19] Fatih Selimefendigil, F. Hakan, Öztop. "Magnetohydrodynamics forced convection of nanofluid in multi-layered U-shaped vented cavity with a porous region considering wall corrugation effects, Int. Commun. Heat Mass Tran. 113 (2020), 104551.
[20] Fatih Selimefendigil, Ali J. Chamkha, Magnetohydrodynamics mixed convection in a power law nanofluid-filled triangular cavity with an opening using Tiwari and Das' nanofluid model, J. Therm. Anal. Calorim. 135 (2019) 419–436.
[21] Fatih Selimefendigil, F. Hakan, Öztop. "Hydro-thermal performance of CNT nanofluid in double backward facing step with rotating tube bundle under magnetic field, Int. J. Mech. Sci. 185 (2020), 105876.
[22] Shahin Shoeibi, Nader Rahbar, Ahad Abedini Esfahlani, Hadi Kargarsharifabad, Application of simultaneous thermoelectric cooling and heating to improve the performance of a solar still: an experimental study and exergy analysis, Appl. Energy 263 (2020), 114581.
[23] Fares, R., Fateh Mebarek-Oudina, A. Aissa, S. M. Bilal, and Hakan F. Öztop. "Optimal entropy generation in Darcy-Forchheimer magnetized flow in a square enclosure filled with silver based water nanoliquid." J. Therm. Anal. Calorim. 147 (2022): 1571-1581.
[24] N. Casson, A flow equation for pigment-oil suspensions of the printing ink type, Rheol. Disperse Syst. (1959) 84–104.
[25] A. Subba Rao, V. Ramachandra Prasad, N. Bhaskar Reddy, O. Anwar Bég, Heat transfer in a Casson rheological fluid from a semi-infinite vertical plate with partial slip, Heat Tran. Asian Res. 44 (2015) 272–291.
[26] R Byron Bird, G.C. Dai, Barbara J. Yarusso, The rheology and flow of viscoplastic materials, Rev. Chem. Eng. 1 (1983) 1–70.
[27] E. Mitsoulis, Flows of Viscoplastic Materials: Models and Computations Rheol, 2007, pp. 135–178.
[28] T. Hayat, S.A. Shehzad, A. Alsaedi, Soret and Dufour effects on magnetohydrodynamic (MHD) flow of Casson fluid, Appl. Math. Mech. 33 (2012) 1301–1312.
[29] Hakan F. Öztop, Patrice Estellé, Wei-Mon Yan, Khaled Al-Salem, Jamel Orfi, Omid Mahian, A brief review of natural convection in enclosures under localized heating with and without nanofluids, Int. Commun. Heat Mass Tran. 60 (2015) 37–44.
[30] M. Mustafa, T. Hayat, I. Pop, Al Aziz, Unsteady boundary layer flow of a Casson fluid due to an impulsively started moving flat plate, Heat Tran. Asian Res. 40 (2011) 563–576.
[31] I.L. Animasaun, Effects of thermophoresis, variable viscosity and thermal conductivity on free convective heat and mass transfer of non-darcian MHD dissipative Casson fluid flow with suction and nth order of chemical reaction, J. Nigerian Math. Soc. 34 (2015) 11–31.
[32] J.P. Garandet, T. Alboussiere, R. Moreau, Buoyancy driven convection in a rectangular enclosure with a transverse magnetic field, Int. J. Heat Mass Tran. 35 (1992) 741–748.
[33] N. Rudraiah, R.M. Barron, M. Venkatachalappa, C.K. Subbaraya, Effect of a magnetic field on free convection in a rectangular enclosure, Int. J. Eng. Sci. 33 (1995) 1075–1084.
[34] H. Ben Hadid, D. Henry, Numerical simulation of convective three-dimensional flows in a horizontal cylinder under the action of a constant magnetic field, J. Cryst. Growth 166 (1996) 436–445.
[35] T. Tagawa, H. Ozoe, Enhancement of Heat Transfer Rate by Application of a Static Magnetic Field During Natural Convection of Liquid Metal in a Cube, 1997, pp. 265–271.
[36] Mikhail Aleksandrovich Sheremet, H.F. Oztop, I. Pop, MHD natural convection in an inclined wavy cavity with corner heater filled with a nanofluid, J. Magn. Magn Mater. 416 (2016) 37–47.
[37] Fatih Selimefendigil, F. Hakan, Öztop. "Corrugated conductive partition effects on MHD free convection of CNT-water nanofluid in a cavity, Int. J. Heat Mass Tran. 129 (2019) 265–277.
[38] Kolsi, Lioua, Fatih Selimefendigil, Kaouther Ghachem, Talal Alqahtani, and Salem Algarni. "Pulsating nanofluid flow in a wavy bifurcating channel under partially active uniform magnetic field effects." Int. Commun. Heat Mass Tran. 133 (2022): 105938.
[39] Fatih Selimefendigil, F. Hakan, Öztop. "Effects of conductive curved partition and magnetic field on natural convection and entropy generation in an inclined cavity filled with nanofluid, Phys. Stat. Mech. Appl. 540 (2020), 123004.
[40] T. Hayat, M.Z. Kiyani, I. Ahmad, M. Ijaz Khan, A. Alsaedi, Stagnation point flow of viscoelastic nanomaterial over a stretched surface, Results Phys. 9 (2018) 518–526.
[41] M. Ijaz Khan, A. Khan Sohail, T. Hayat, A. Alsaedi, Entropy optimization in magnetohydrodynamic flow of third-grade nanofluid with viscous dissipation and chemical reaction, Iran. J. Sci. Technol. Trans. A-Science 43 (2019) 2679–2689.
[42] M. Ijaz Khan, Mehr Nigar, Tasawar Hayat, and Ahmed Alsaedi. "On the numerical simulation of stagnation point flow of non-Newtonian fluid (Carreau fluid) with Cattaneo-Christov heat flux, Comput. Methods Progr. Biomed. 187 (2020), 105221.
[43] M. Khan, Waleed Ahmad, M. Ijaz Khan, Tasawar Hayat, Alsaedi Ahmed, Numerical solution of MHD flow of power law fluid subject to convective boundary conditions and entropy generation, Comput. Methods Progr. Biomed. 188 (2020), 105262.
[44] M. Ijaz Khan, Tehreem Nasir, Tasawar Hayat, Niaz B. Khan, Alsaedi Ahmed, Binary chemical reaction with activation energy in rotating flow subject to nonlinear heat flux and heat source/sink, J. Comput. Design Eng. 7 (2020) 279–286.
[45] Yu-Ming Chu, Nargis Khan, M. Ijaz Khan, Kamel Al-Khaled, Nasreen Abbas, Sami Ullah Khan, Muhammad Sadiq Hashmi, Sumaira Qayyum, S. Kadry, Thermophoresis particle deposition analysis for nonlinear thermally developed flow of Magneto-Walter's B nanofluid with buoyancy forces, Alex. Eng. J. 60 (2021) 1851–1860.
[46] Mubbashar Nazeer, Farooq Hussain, Sadia Iftikhar, Muhammad Ijaz Khan, K. Ramesh, Nasir Shehzad, Afifa Baig, Seifedine Kadry, Yu-Ming Chu, Mathematical modeling of bio-magnetic fluid bounded within ciliated walls of wavy channel, Numer. Methods Part. Differ. Equ. (2021), https://doi.org/10.1002/num.22763.
[47] Hussain, Shafqat, Shahin Shoeibi, and Taher Armaghani. "Impact of magnetic field and entropy generation of Casson fluid on double diffusive natural convection in staggered cavity." Int. Commun. Heat Mass Tran. 127 (2021): 105520.
[48] M. Kamran Alam, K. Bibi, A. Khan, S. Noeiaghdam, Dufour and Soret effect on viscous fluid flow between squeezing plates under the influence of variable magnetic field, Mathematics 9 (2021) 2404, https://doi.org/10.3390/math9192404.
[49] M.S. Khan, S. Mei, Shabnam, U. Fernandez-Gamiz, S. Noeiaghdam, S.A. Shah, A. Khan, Numerical analysis of unsteady hybrid nanofluid flow comprising CNTs-ferrousoxide/water with variable magnetic field, Nanomaterials 12 (2022) 180, https://doi.org/10.3390/nano12020180.
[50] M.S. Khan, S. Mei, Shabnam, U. Fernandez-Gamiz, S. Noeiaghdam, A. Khan, S. A. Shah, Electroviscous effect of water-base nanofluid flow between two parallel disks with suction/injection effect, Mathematics 10 (2022) 956, https://doi.org/10.3390/math10060956.
[51] J.V. Tawade, C.N. Guled, S. Noeiaghdam, U. Fernandez-Gamiz, V. Govindan, S. Balamuralitharan, Effects of thermophoresis and Brownian motion for thermal and chemically reacting Casson nanofluid flow over a linearly stretching sheet, Result Eng. 15 (2022), 100448, https://doi.org/10.1016/j.rineng.2022.100448.